Physics of Fluids

Role of barriers in the airborne spread of virus-containing droplets: A study based on high-resolution direct numerical simulations

Cite as: Phys. Fluids **34**, 015104 (2022); https://doi.org/10.1063/5.0072840
Submitted: 25 September 2021 • Accepted: 16 November 2021 • Published Online: 05 January 2022

M. Cavaiola, S. Olivieri, J. Guerrero, et al.

Physics of Fluids ARTICLE scitation.org/journal/phf

Role of barriers in the airborne spread of virus-containing droplets: A study based on high-resolution direct numerical simulations

Cite as: Phys. Fluids **34**, 015104 (2022); doi: 10.1063/5.0072840
Submitted: 25 September 2021 · Accepted: 16 November 2021 ·
Published Online: 5 January 2022

View Online Export Citation CrossMark

M. Cavaiola,[1,2,a] S. Olivieri,[3] J. Guerrero,[1] A. Mazzino,[1,2] and M. E. Rosti[3]

AFFILIATIONS

[1]Department of Civil, Chemical and Environmental Engineering (DICCA), University of Genova, Via Montallegro 1, 16145 Genova, Italy
[2]INFN, Genova Section, Via Montallegro 1, 16145 Genova, Italy
[3]Complex Fluids and Flows Unit, Okinawa Institute of Science and Technology Graduate University, 1919-1 Tancha, Onna-son, Okinawa 904-0495, Japan

[a]Author to whom correspondence should be addressed: mattia.cavaiola@edu.unige.it

ABSTRACT

State-of-the-art direct numerical simulations are exploited to study the role of barriers on the airborne spread of virus-containing droplets. Our study is motivated by recent findings pointing to the key role of turbulence in dictating the final fate of virus-containing droplets in violent human exhalations. Here, all active scales of motion have been explicitly taken into account, including their interplay with the droplet evaporation process occurring once droplets are emitted in a drier ambient air, and accounting for the time-varying droplet inertia due to the water loss via evaporation. We show that barriers commonly used to mitigate the airborne spread of the virus cause nontrivial dynamical effects influencing the final reach of the virus-containing droplets, not always being beneficial to this aim. These conclusions do depend on the relative humidity of the ambient condition, and in particular whether the ambient humidity is above or below the so-called efflorescence relative humidity. Our findings provide a physically based answer to the question on how effective barriers are to protect people from airborne virus transmission in indoor environments.

I. INTRODUCTION

The airborne transmission of virus-containing respiratory droplets exhaled during coughing or sneezing, or even talking and breathing, represents a problem of paramount importance in light of the recent COVID-19 pandemic.[1,2] Recently, numerous studies have been performed to better understand the essential mechanisms of airborne transmission.[3–11] Furthermore, investigations have considered various real-life situations and addressed several aspects related to open space and indoor environments.[12–16]

Particular attention has been paid to characterizing the role of ambient humidity in determining the lifetime of virus-containing droplets.[11,17–19] This is a crucial aspect since the evaporation rate of saliva droplets depends on environmental conditions, such as the ambient temperature and relative humidity, as well as other physical properties (e.g., droplet size and composition).[20]

Another key feature governing the lifetime of saliva droplets is fluid turbulence. Exploiting state-of-the-art direct numerical simulations (DNSs), it has been recently shown that turbulent fluctuations within the puff of exhaled humid air play a crucial role in determining the evaporation time.[21] In particular, numerical simulations conducted with two different coarse-graining techniques (i.e., filtered DNS and mean-field simulation), when compared with results from fully resolved DNS, show that using coarse-graining techniques leads one to strongly underestimate the droplet evaporation time with a strong impact on the prediction of the final reach of virus-containing droplets.

In order to prevent the spread of the disease, the World Health Organization (WHO) suggested a series of actions, such as social distancing, surface disinfection, room ventilation, and the use of face masks and barriers, especially in indoor environments. Social distancing prevents direct contact among individuals and can reduce the potential airborne transmission of virus-containing droplets. In scientific literature, however, a relatively large dispersion of data concerning the recommended safe distance can be found, ranging from 1 to

8 m.[16,22–24] Indeed, the currently available information is inadequate to design social distancing recommendations on a solid scientific basis, with remarkably different predictions depending on the assumed initial droplet size distribution and ambient conditions.[11] On the other hand, several studies have analyzed the efficiency of face masks as devices to minimize the risk of infection via aerial transmission.[25–28] A variety of commonly available mask types has been compared, observing that some mask types approach the performance of standard surgical masks, while some mask alternatives, such as neck gaiters or bandanas, offer very little protection.[29]

Barriers are often used to protect individuals within indoor environments. Numerous devices have been developed and deployed in an effort to protect healthcare workers during high-risk procedures, and in indoor workplaces to protect employees and customers. However, only a few studies have thoroughly and quantitatively examined their impact on the dispersion of droplets and aerosols.[30,31] The available results show that the placement of large transparent plastic sheets over patients' faces can limit the contamination area,[32] showing that such protective tools are helpful in decreasing the contamination from droplet dispersion.[33] However, to the best of our knowledge, no studies based on a DNS approach are reported in the current literature.

To make a step forward in characterizing the efficacy of barriers in the mitigation of airborne transmission, DNSs of the unsteady turbulent puff carrying many virus-containing droplets represent a valuable tool of analysis. Such a high-fidelity computational approach has been recently employed to unravel the essential physical mechanisms involved in the transport and evaporation of virus-containing exhaled droplets.[11,21] Here, we employ this computational tool to analyze a variety of geometrical and ambient conditions, along with deducing the optimal distance minimizing the reach of exhaled droplets.

The rest of this paper is structured as follows: Sec. II presents the governing equations and numerical method, Sec. III shows the main results, and Sec. IV draws the main conclusions.

II. NUMERICAL METHOD

The fluid flow is governed by the well-known Oberbeck–Boussinesq equations (i.e., the set of the incompressible Navier–Stokes equations coupled to the advection–diffusion equation for the temperature field) given by[34]

$$\partial_t \boldsymbol{u} + \boldsymbol{u}\cdot\boldsymbol{\partial}\boldsymbol{u} = -\frac{1}{\rho}\boldsymbol{\partial} p + \nu\partial^2\boldsymbol{u} - \beta\boldsymbol{g}(T - T_a), \tag{1}$$

$$\boldsymbol{\partial}\cdot\boldsymbol{u} = 0, \tag{2}$$

$$\partial_t T + \boldsymbol{u}\cdot\boldsymbol{\partial} T = \kappa\partial^2 T, \tag{3}$$

where $\boldsymbol{u}(\boldsymbol{x},t)$ and $p(\boldsymbol{x},t)$ are the fluid (here air) velocity and pressure fields, respectively; ν, ρ, and β are the (constant) kinematic viscosity, density and thermal expansion coefficient of the air, respectively; $\boldsymbol{g} = (0,0,-g)$ is the gravitational acceleration; $T(\boldsymbol{x},t)$ is the puff temperature field and T_a is the (constant) quiescent ambient temperature; finally, κ is the air thermal diffusion coefficient. Air exhaled by humans is rich in water vapor, thus the specific humidity q is modeled by the advection–diffusion equation as follows:[35]

$$\partial_t q + \boldsymbol{u}\cdot\boldsymbol{\partial} q = D_v\partial^2 q, \tag{4}$$

where D_v is the water vapor diffusivity. In human exhalations $q \ll 1$, and we obtain $q \sim r \sim e\varepsilon/p_a$, where r is the mixing ratio, e is the water vapor pressure, p_a is the ambient pressure, and ε is the ratio between the molar mass of water vapor and molar mass of dry air.[35] From the above relationships, it then follows that the supersaturation field is $s = e/e_{sat} - 1 \sim r/r_{sat} - 1$, where the subscript "sat" denotes the value at saturation. Exploiting the Magnus–Tetens relationship between e_{sat} and T (in which the temperature T is in °C, see Ref. 36), one immediately gets the supersaturation field s from the integration of the advection–diffusion equation given by Eq. (4) for q.

Respiratory droplets are modeled as an ensemble of N spherical particles of radius R_i dispersed within the expiratory airflow. Each droplet is individually described by the following well-known set of equations:[37]

$$\dot{\boldsymbol{X}}_i = \boldsymbol{U}_i(t) + \sqrt{2D_v}\boldsymbol{\eta}_i(t), \tag{5}$$

$$\dot{\boldsymbol{U}}_i = \frac{\boldsymbol{u}(\boldsymbol{X}_i(t),t) - \boldsymbol{U}_i(t)}{\tau_i} + \boldsymbol{g}, \tag{6}$$

for $i = 1,\ldots,N$, and where $\boldsymbol{X}_i$ and $\boldsymbol{U}_i$ are the position and velocity vectors of the ith droplet, respectively. Note that, for coughing events, the backreaction to the carrier airflow can be safely neglected in light of the negligible volume fraction (always smaller than 10^{-5}, see Refs. 38 and 39). The dynamics is affected by a Brownian white-noise process $\boldsymbol{\eta}_i$ and by the Stokes time $\tau_i = 2(\rho_{Di}/\rho_a)R_i^2(t)/9\nu_a$. In order to define the density of the ith droplet ρ_{Di}, we assume the droplet to be composed of a dry nucleus with density ρ_N surrounded by a salty water layer with density ρ_w. The dry nucleus is composed of a soluble phase (NaCl) and a insoluble phase (mucus), giving an overall density, which can be expressed as

$$\rho_N = \frac{\rho_u}{1 - \varepsilon_m[1 - (\rho_u/\rho_s)]}, \tag{7}$$

where ε_m is the mass fraction of the soluble material (NaCl) with respect to the total dry nucleus and ρ_u and ρ_s are the density of the insoluble (mucus) and soluble (NaCl) parts, respectively. Thus, the density ρ_{Di} of the droplet can be computed as

$$\rho_{Di} = \rho_w + (\rho_N - \rho_w)\left(\frac{r_{Ni}}{R_i(t)}\right)^3, \tag{8}$$

where the radius of the (dry) solid part of the droplet when NaCl is totally crystallized is given by

$$r_{Ni} = R_i(0)\left(\frac{\mathscr{C}\,\rho_w}{\mathscr{C}\,\rho_w + \rho_N(1-\mathscr{C})}\right)^{1/3}, \tag{9}$$

with $\mathscr{C}$ being the mass fraction of dry nucleus with respect to the total droplet. Finally, the droplet radius R_i evolves according to a condensation model that has been successfully employed in the analysis of rain formation processes,[40–43] i.e.,

$$\frac{d}{dt}R_i^2(t) = 2C_R\left(1 + s(\boldsymbol{X}_i(t),t) - e^{\frac{A}{R_i(t)} - B\frac{r_{Ni}^3}{R_i^3(t) - r_{Ni}^3}}\right), \tag{10}$$

where C_R is the droplet condensational growth rate defined as

$$C_R = \left[\frac{\rho_w R_v\,(273.15 + T_a)}{e_{sat}\,D_v} + \frac{\rho_w L_w^2}{k_a R_v\,(273.15 + T_a)^2} - \frac{\rho_w L_w}{k_a(273.15 + T_a)}\right]^{-1}, \tag{11}$$

and A and B are two model parameters given by

$$A = \frac{2\sigma_w}{R_v(T_a + 273.15)\rho_w} \quad \text{and} \quad B = \frac{n_s \Phi_s \varepsilon_v M_w \rho_s}{M_s \rho_w}, \tag{12}$$

where $\varepsilon_v = \varepsilon_m(\rho_N/\rho_s)$ is the volume fraction of the dry nucleus with respect to the total droplet. The water saturation vapor pressure is given by[36]

$$e_{sat} = 6.1078 \times 10^2 \, e^{(17.27T_a/(T_a+237.3))} \text{ Pa}. \tag{13}$$

Note that, also in this case, in Eqs. (11)–(13) the temperature T_a is expressed in degrees Celsius. The values of the physical and chemical parameters selected for the present study are provided in Table II in the Appendix.

The initial droplet size distribution is the well-known distribution from Duguid,[44] with droplet radii approximately ranging from 1 to 1000 μm and the 95% falling between 1 and 50 μm. Droplets are set initially at rest and randomly distributed within a sphere of radius 1 cm located inside the circular pipe from which the exhaled airflow is released; in our simulations, we assume the initial temperature of the exhaled air to be equal to 30 °C, as in Ref. 45. Finally, the exhaled droplets enter the ambient air initially at rest with a relative humidity RH_a. Note that, states of local equilibrium are possible owing to the solute effect.[40]

Figure 1 shows a sketch of the geometrical setup employed in our simulations. We consider a domain box of length $L_x = 3$ m, width $L_y = 2$ m, and height $L_z = 3$ m. The size of the numerical domain has been chosen in order to represent a typical room. The center of the barrier is placed at 1.6 m from the ground, having a height of 0.5 m. The distance d of the barrier from the mouth is varied together with the ambient relative humidity. The fluid is initially at rest, i.e., $\boldsymbol{u}(\boldsymbol{x}, 0) = \boldsymbol{0}$, and at the ambient supersaturation $s(\boldsymbol{x}, 0) = s_a = \text{RH}_a - 1$. The exhaled air is assumed to be fully saturated[45] (i.e., $s_{\text{mouth}} = 0$) and is injected through a round opening of area $A_{\text{mouth}} = 4.5$ cm^2 mimicking the mouth, at a distance from the ground of $z_{\text{mouth}} = 1.6$ m. The injected airflow is along the horizontal direction and it is prescribed according to the experimental measurements reported by Gupta *et al.*[46] The duration of exhalation is around 0.5 s with a peak velocity of 13 m/s, corresponding to a Reynolds number (based on the peak velocity and on the mouth average radius) of about 9×10^3. For the other domain boundaries, we prescribe the no-slip condition to simulate the presence of the body and the flow inside a closed room at the bottom ($z = 0$), top ($z = L_z$) and left ($x = 0$) boundaries. For both the velocity and supersaturation field, we impose a convective outlet boundary condition at the right boundary ($x = L_x$). Finally, periodic boundary conditions are enforced in the spanwise direction (i.e., $y = 0$ and $y = L_y$). In our simulations, all the droplets that hit on surfaces remain attached to them.

The governing equations are solved numerically using the in-house code *Fujin* (https://groups.oist.jp/cffu/code). The equations for the fluid flow are discretized with the (second-order) central finite-difference method in space and the (second-order) Adams–Bashfort scheme in time. A fast and efficient FFT-based approach is used to solve the resulting Poisson equation for pressure. The droplet dynamic equations given by Eqs. (5), (6), and (10) are advanced in time using the explicit Euler scheme. The code has been extensively validated in a variety of problems[47–52] and already employed for the simulation of expiratory events.[11,21,53] To model the presence of the barrier, here we use the immersed boundary method (IBM) originally proposed by Kajishima *et al.*[54] For the present simulations, the numerical domain is discretized with uniform grid spacing $\Delta x = 1.75$ mm in all directions, resulting in a total number of approximately 1.2 billion grid points. The convergence of the results was verified by comparing the results with those obtained by doubling the grid resolution.[11]

Exploiting such a DNS approach, ten numerical simulations were performed for five possible barrier configurations at two different environmental conditions. Specifically, we consider a barrier with a height of 0.5 m, which extends indefinitely along the spanwise direction, and vary the distance from the mouth at which the barrier is placed. Five geometrical configurations are considered: barrier placed at 0.25 0.5, 0.75, 1 m from the mouth, and the configuration without any barrier for the sake of comparison. For each barrier, we consider two different values of ambient relative humidity, "dry" and "wet,"

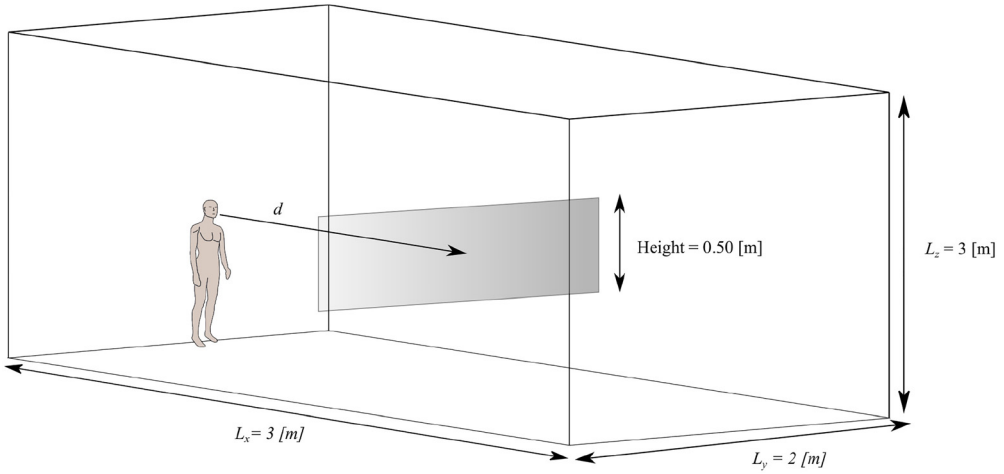

FIG. 1. Sketch of the geometrical setup employed in our study.

corresponding to $RH_a = 30$ and $RH_a = 60$, respectively. In the wet condition, droplets do not evaporate completely but remain in equilibrium with the surrounding environment. In contrast, in the dry condition all droplets evaporate completely and shrink to their dry nuclei.

To assess the associated risk of transmission, we quantify the viral load carried by the exhaled droplets, by tracking the position of each droplet for a time of 15 s. As done in Refs. 11 and 21, we quantify these observations by defining the (relative) viral load (VL) of the ith droplet as the ratio between its initial volume and the cumulative initial volume of all exhaled droplets. By assuming an initial size distribution of the exhaled droplets,[44] we are interested in analyzing the role of the barrier in removing the VL from air, and how the presence of the barrier can modify the sedimentation pattern of the VL to the ground. In Figs. 2 and 3, we show three representative cases of the virus-containing droplets exhaled during a cough, with and without barrier in front of the mouth. The trajectories of the droplets and their final reach are strongly modified by the presence of the barrier; as a consequence, it is expected that the same is true for the amount of viral load settling to the ground and that remaining in the air.

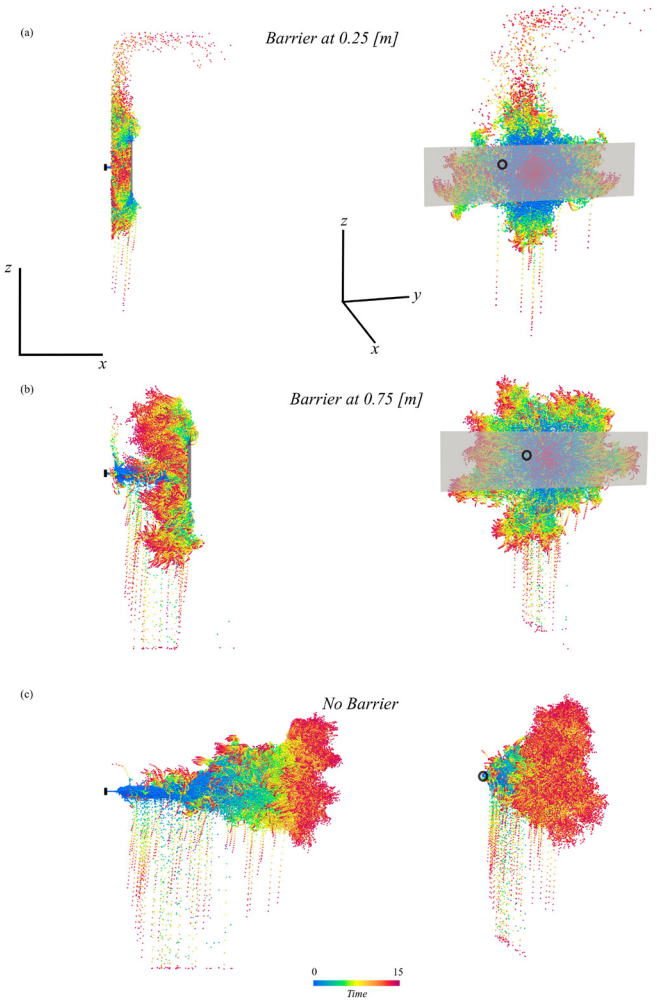

FIG. 2. Side (left panels) and 3D (right panels) views of virus-containing droplet trajectories computed by means of high-resolution DNS for three representative configurations, i.e., with barrier placed at a distance of (a) 0.25 and (b) 0.75 m from the mouth and (c) without barrier. Results are shown for the dry condition. Droplets are colored according to their time instant to which they are found in space. The black bar, on the left panel, and the black circle, on the right panel, indicate the exhalation origin.

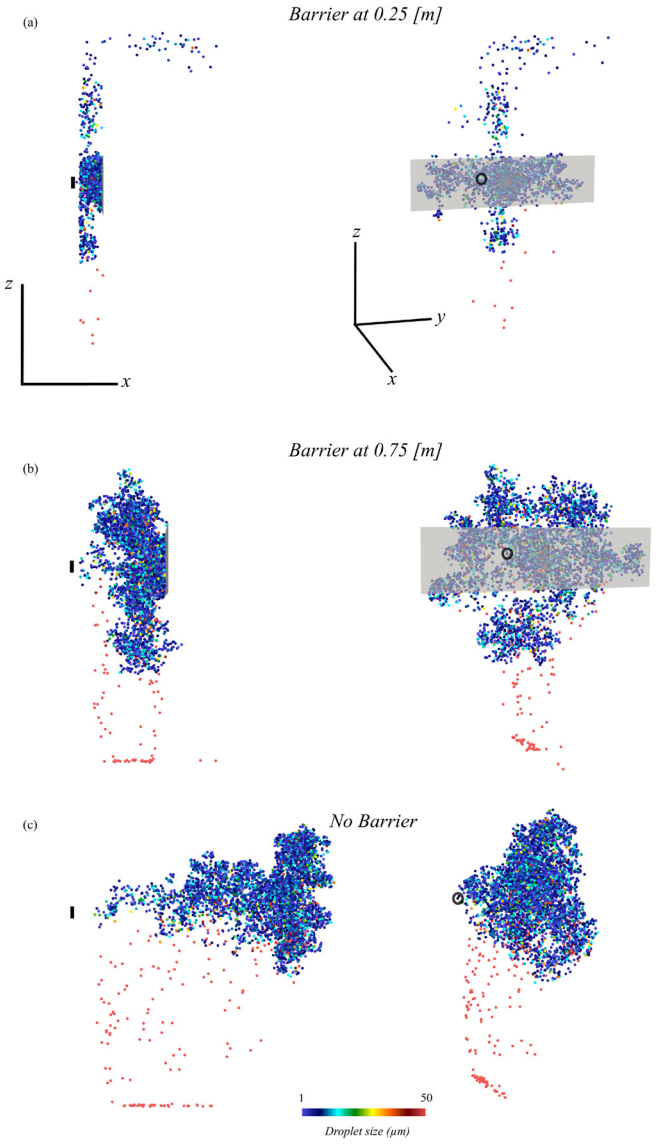

FIG. 3. Side (left panels) and 3D (right panels) views of the position of the virus-containing droplets at the final observation time (15 s) for three representative configurations, i.e., with barrier placed at a distance of (a) 0.25 and (b) 0.75 m from the mouth and (c) without barrier. Results are shown for the dry condition. The black bar, on the left panel, and the black circle, on the right panel, indicate the exhalation origin. Droplets are colored by their radius size (μm). Note that the color bar shows a range between 1 and 50μm to emphasize differences between small ($1\ \mu\text{m} \leq R_i \leq 50\ \mu\text{m}$) and large ($R_i > 50\ \mu\text{m}$) droplets.

TABLE I. Cumulative viral load (*VL*) and number of droplets (*ND*) on the barrier, on the ground, and remaining in the air, for the two ambient humidities considered.

Barrier distance	*VL* on barrier (%)	*VL* to ground (%)	*VL* in air (%)	*ND* on barrier (%)	*ND* to ground (%)	*ND* in air (%)
Dry, 0.25 m	98.91	0.32	0.77	47	1.57	51.43
Dry, 0.5 m	95.15	3.24	1.61	32.38	0.66	66.96
Dry, 0.75 m	19.22	78.15	2.63	17.81	0.97	81.22
Dry, 1 m	3.78	92.54	3.68	5.35	1.13	93.52
Dry, no barrier	0	95.81	4.19	0	1.11	98.89
Wet, 0.25 m	29.3	70.64	0.06	67.3	1	31.7
Wet, 0.5 m	14.46	85.26	0.27	45.13	1.42	53.45
Wet, 0.75 m	6	93.57	0.43	22.6	3.08	74.32
Wet, 1 m	1.38	98.1	0.52	8.39	4.64	86.97
Wet, no barrier	0	99.43	0.57	0	5.05	94.95

III. RESULTS

In order to quantify the spread of virus-containing droplets in indoor environments where a barrier is present (Fig. 1), we study the evolution of viral load that settles to the ground, that deposits on the barrier, and that remains airborne. In accounting for the airborne viral load, we neglect all the droplets that stick on surfaces such as the barrier and the ground. Moreover, in our simulations we did not find any droplet attached on the top and body surface, i.e., at $L_z = 3$ m and $x = 0$ m, respectively. Table I reports a summary of the cumulative *VL* after the overall simulation time (15 s), separating the contribution collected on the barrier, that settling to the ground, and that remaining in the air, together with the corresponding number of droplets normalized to the total number of droplets (ND). Note however that the latter quantity can be misleading because of the presence of a few of the biggest droplets carrying the largest part of the viral load. For example, the following holds in the case of the barrier at a distance of 0.25 m from the mouth: in the dry condition, almost 47% of the droplets impact on the barrier carrying a *VL* of 98.9%; in the wet case instead, 67% of the droplets impact on the barrier, yet representing only 29% of the *VL*. From Table I, it is possible to observe small differences between the dry and wet cases in terms of the number of droplets reaching the ground (1% and 1.57%, respectively), while large differences are evident for the carried viral load, 0.32% and 70%, respectively.

Differences between the dry and wet conditions can be found when evaluating the distance from the mouth traveled by the droplets. Figure 4 shows the probability density function (*pdf*) of the horizontal distance traveled by the droplets when they reach the ground. For the two ambient conditions, we count the number of settled droplets at time 15 s, comparing the results for different distances of the barrier from the mouth. The effect of the barrier is particularly significant in the cases where it is closer to the mouth, where the largest amount of droplets settles within 0.1 and 0.5 m, respectively, for both the dry and wet conditions. When the barrier is present, it is also possible to note the effect of the ambient humidity that allows the droplets to travel for a larger distance in the wet condition with respect to the dry condition. This is in contrast with the cases without barrier, where the droplets are found to travel for larger distances in the dry condition. This is a clear inertial effect of the larger droplets: in the wet condition droplets are typically heavier than in the dry condition and follow ballistic trajectories, thus being able to overcome the barrier from below. On the other hand, the light droplets of the dry condition behave essentially as fluid tracers, thus remaining trapped in the vortical structures generated by the presence of the barrier (see Fig. 2).

To complement this analysis, in Figs. 5(a) and 5(b) we show the cumulative *VL* settling to the ground as a function of the distance from the mouth. We compare the settled *VL* with different distances of the barrier from the mouth, superimposing the case without barrier for the sake of comparison, for the dry and wet conditions. It is possible to notice the effect of the barrier in determining the amount of *VL* that reaches the ground: by increasing the distance of the barrier, the settling *VL* grows, for both the dry and wet ambient conditions. As expected, a higher amount of *VL* reaches the ground for the wet condition, especially when the barrier is close to the mouth (barrier distance of 0.25 and 0.5 m). By looking at the wet condition in Fig. 5(b), we observe that the presence of the barrier has a negligible influence on the amount of settled *VL* when the barrier is far from the mouth, e.g., 0.75 and 1 m. Moreover, a greater distance is traveled by the *VL* in the wet condition with respect to the dry condition when the barrier is

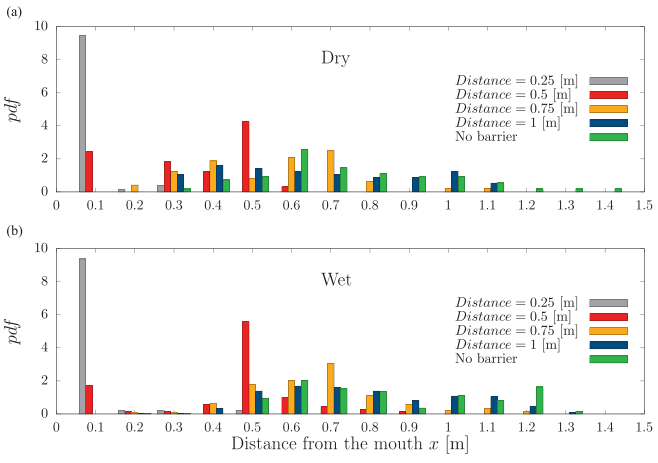

FIG. 4. Probability density function of the distance from the mouth when droplets reach the ground. (a) Dry condition and (b) wet condition.

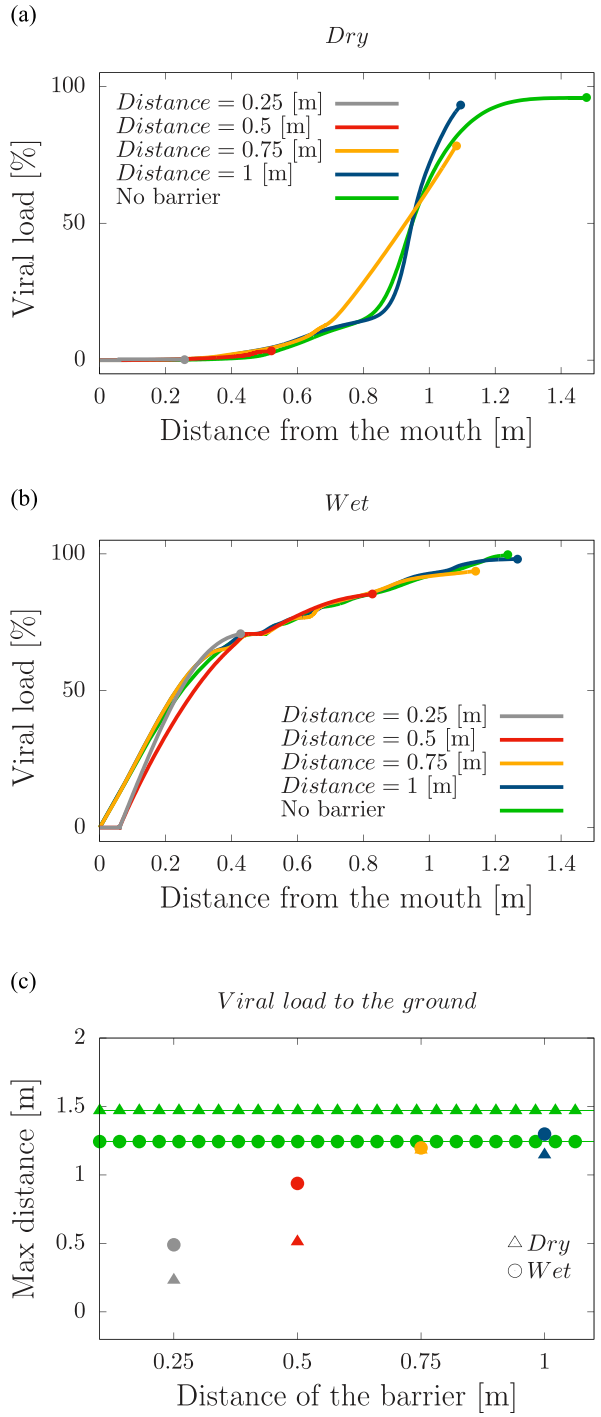

FIG. 5. Cumulative viral load settling to the ground (%) as a function of the distance from the mouth: (a) dry and (b) wet conditions. The gray line represents the case with the barrier at 0.25 (m), the red line at 0.5 (m), the yellow line at 0.75 (m), the blue line at 1 (m), and the green line the case without barrier. The dots at the end of the lines indicate the maximum distance reached by the cumulative viral load. (c) Maximum distance reached by the cumulative settling viral load in the (triangles) dry and (circles) wet conditions. The green point lines indicate the cases without barrier.

present. In Fig. 5(c), we quantify the maximum distance reached by the *VL* settled to the ground; except for the case of the barrier at a distance of 0.75 m, where the maximum distance is almost the same between the two ambient humidities; the wet condition always shows a higher maximum distance.

A study of the distance traveled by droplets and viral load is important to define protocols and rules to protect people living in indoor environments. Studying the time history of the exhaled viral load during a cough is another important issue in order to quantify how long the viral load takes to settle and to impact on the barrier. In Fig. 6, we show the cumulative *VL* settling to the ground, that was captured by the barrier, and that remaining airborne, for the observation time of 15 s, for the dry and wet ambient conditions. Especially for the dry condition, the role of the barrier is crucial when it is close to the mouth, where almost 99% of the *VL* is captured in less than 1 s [Figs. 6(a) and 6(b)]. This is not the case for the wet condition, where with a barrier at a distance of 0.25m and 0.5m from the mouth, only 29% and 15% of the *VL* is captured by the barrier, respectively, in less than 1 s [Figs. 6(e) and 6(f)]. As far as the airborne viral load is concerned, we found a lower residence time in the air for the dry condition (less than 1 s), in comparison with the wet condition where instead it is almost 1 s [Figs. 6(a) and 6(e)]. By placing the barrier at increasing distances from the mouth, the captured *VL* reduces progressively. The amount of *VL* remaining in the air increases more for the dry cases, with longer residence time with respect to the wet ones, where the majority of *VL* is lost by sedimentation [Figs. 6(b)–6(d) and 6(f)–6(h)]. Considering a barrier at a distance of 0.75 m from the mouth, we find 6% of the airborne *VL* after 6 s for the dry condition, while it is 0.57% for the wet one. Also, one can observe the negligible effect of the barrier when it is at 1m from the mouth [Figs. 6(d) and 6(h)]. This is more evident for the wet condition, where the curves are substantially superimposed compared to those for the cases without barrier [Fig. 6(h)].

Once the viral load is removed from the air by sedimentation or from the impact with the barrier, the remaining viral load is still airborne and can play a crucial role in disease transmission, such as COVID-19 infection.[4] Thus, in the last step of our analysis we focus on the distance traveled by the airborne viral load. In Figs. 7(a) and 7(b), we report the cumulative airborne *VL* as a function of distance from the mouth, for the two ambient conditions considered. For both the dry and wet conditions, the barrier has an important role in determining the distance traveled by the airborne *VL*, also when the barrier is far from the mouth; this distance is always lower with respect to the case when the barrier is not present, where the *VL* can travel more than 2 m from the mouth. Indeed, the traveled distance is approximately 1.3 and 1 m for the dry and wet conditions with the barrier at 1 m from the mouth. Of particular interest is the role of the distance of the barrier in determining the distance traveled by the airborne viral load: by displacing the barrier away from the mouth, the traveled distance increases; however, when the barrier is very close to the mouth (0.25 m), the distance traveled is higher than in the other cases (0.5, 0.75, and 1 m) for both dry and wet conditions. This can be appreciated from Fig. 2(a), where the presence of the barrier determines an upward flow velocity, which carries the lightest droplets above the barrier and then lets them travel beyond for larger distances. We quantify the maximum distance reached by the airborne viral load in the observation time in Fig. 7(c). Also here, we can note the nontrivial effect of the barrier when it is at a distance of 0.25 m, where the airborne viral load travels for large

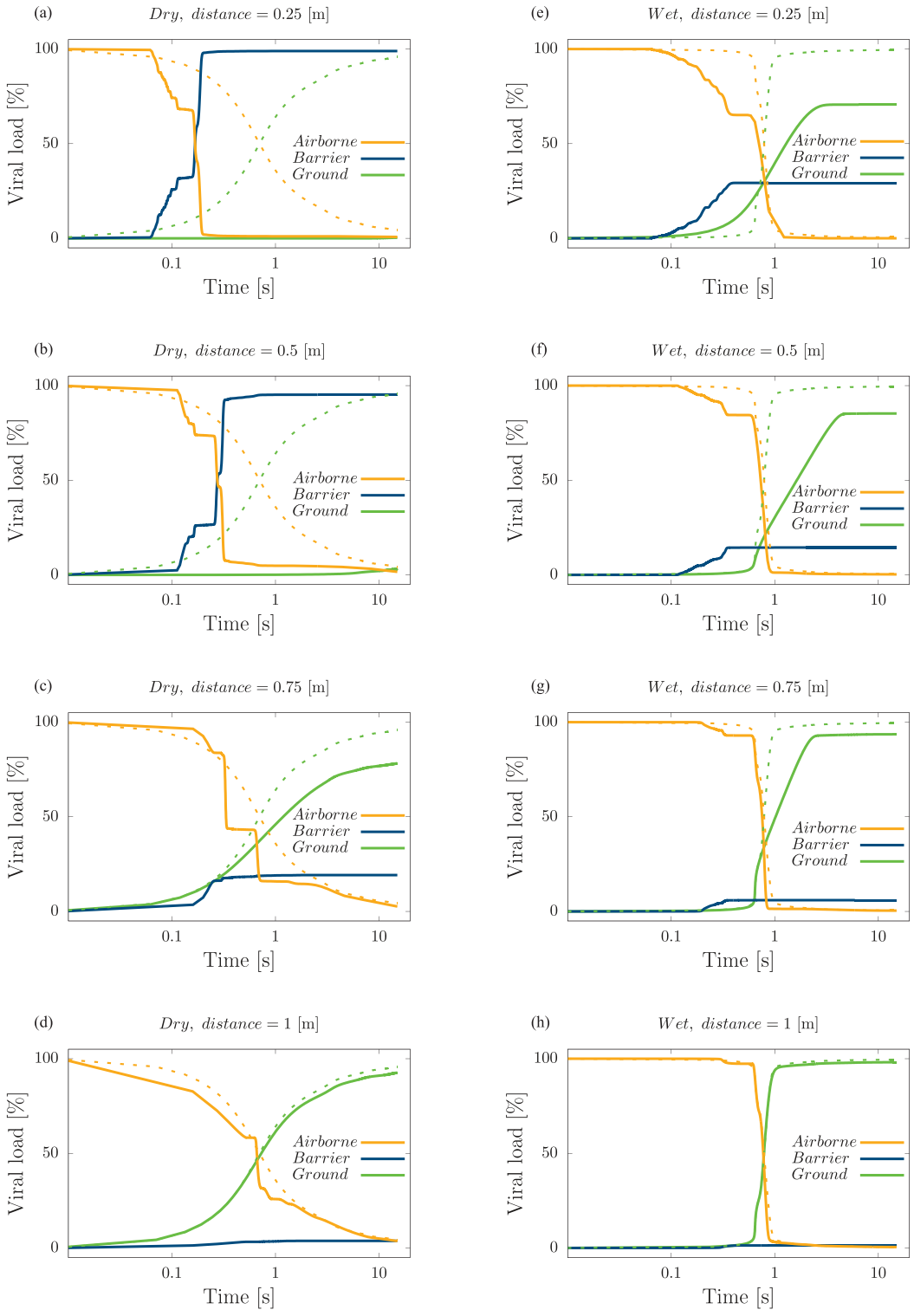

FIG. 6. Time history of the cumulative viral load settling to the ground (green), captured by the barrier (blue) and remaining airborne (yellow). For the sake of comparison, we include the results for the case without barrier (dashed lines of the same colors). The different barrier distances and ambient humidities are reported: (a) $d = 0.25$ m dry, (b) $d = 0.5$ m dry, (c) $d = 0.75$ m dry, (d) $d = 1$ m dry, (e) $d = 0.25$ m wet, (f) $d = 0.5$ m wet, (g) $d = 0.75$ m wet and (h) $d = 1$ m wet.

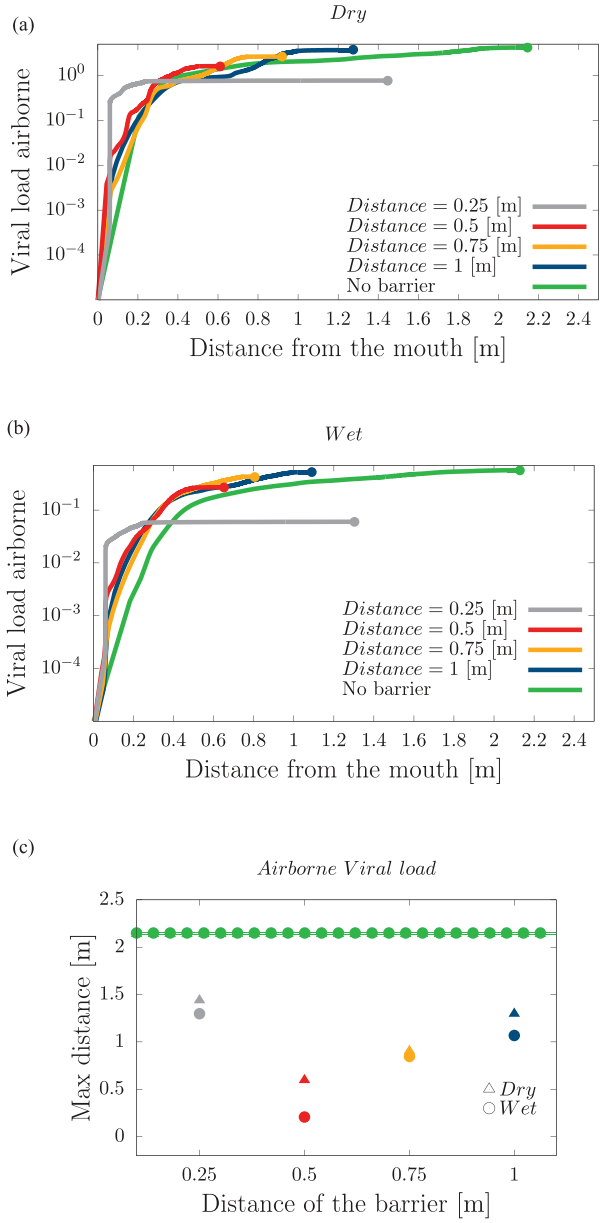

FIG. 7. Cumulative airborne viral load (%) as a function of distance from the mouth (a) for the dry and (b) wet conditions. The gray line represents the case with the barrier at a distance from the mouth of 0.25 (m), the red line at 0.5 (m), the yellow line at 0.75 (m), the blue line at 1 (m), and the green line for the case without barrier. The dots at the end of the lines indicate the maximum distance reached by the cumulative viral load. (c) Maximum distance reached by the cumulative airborne viral load in the (triangles) dry and (circles) wet conditions. The green point lines indicate the cases without barrier.

distance beyond the barrier, more than in the other cases. Finally, due to the lighter weight of the droplets in the dry conditions, the maximum distance is always greater than what we observe in the wet conditions, except for the case with a barrier at 0.75 m where the maximum distance is approximately the same for the two conditions considered.

IV. CONCLUSIONS

We performed numerical simulations exploiting state-of-the-art DNS to investigate the role of barriers as protection devices from the viral load exhaled during a cough. We considered two values of ambient relative humidity denoted, in short, by dry and wet ($RH_a = 30$ and $RH_a = 60$, respectively), and four distances of the barrier from the mouth (0.25, 0.5, 0.75, and 1 m), comparing the obtained results with the case without barrier. By assuming a representative initial size distribution[44] of the exhaled droplets, we quantified the viral load of each droplet and we tracked them in space and in time (up to 15 s).

We analyzed the distance traveled by the viral load from the mouth, and we determined the *VL* amount settling to the ground and that remaining airborne. For all the barrier distances investigated, in the wet case, the settling viral load travels for larger distances compared to the dry condition. This result has been interpreted as a manifestation of the larger inertia of droplets in the wet case causing ballistic events during the transport process. This fact is in contrast with the observation in the case without barrier, where, as expected and in agreement with Ref. 11, it is the dry case that allows the *VL* to settle further away from the mouth. Since the lightest droplets behave as fluid tracers, they remain trapped in the vortices created by the exhaled flow impacting on the barrier, thus making it difficult to travel for larger distances. This is the main mechanism caused by the barrier as a protection device. Indeed, we observe a greater amount of viral load captured by the barrier in the dry case, especially when it is close to the mouth with a barrier distance of 0.25 m. In this case, the captured viral load is approximately 99% with respect to the 30% observed in the wet case. On the other hand, moving away the barrier from the mouth makes the captured viral load increasingly small. Moreover, we observe that the residence time in the air increases more in the dry than in the wet condition. When the barrier is far from the mouth, it has a negligible effect as a protection device, and this is more evident in the wet condition than in the dry one.

Another important focus of our work is on the airborne viral load. Since this fraction of viral load does not settle (within the investigated observation time) and it is not captured by the barrier, it may contribute to spread the infection, also by various means, e.g., building ventilation systems. Our results show a larger amount of airborne viral load for cases in the dry condition, which increases with the distance of the barrier from the mouth. The barrier has therefore an important role to limit the distance traveled by the airborne *VL*, since it is always smaller than that in the case without barrier. Furthermore, the dry cases show a greater distance traveled from the mouth compared to the wet cases. For the two ambient humidities here considered, the particular configuration when the barrier is placed very close to the mouth (i.e., 0.25 m) generates a flow field that allows the lightest droplets to travel far away from the barrier by passing above it.

It is necessary to point out that the results described in this work are characteristic of the dimensions used to represent a typical room where the ceiling is at a height of 3 m. Considering a room with different sizes than those used here, the results may vary especially from a quantitative point of view. Nevertheless, we provide a general framework for characterizing the efficacy of barriers in the mitigation of airborne transmission, and the obtained results can actively contribute to select optimal strategies of protection within indoor environments. Furthermore, our results are not restricted to COVID-19, but can be extended to all the infections where the main transmission route is via airborne virus-containing droplets.

ACKNOWLEDGMENTS

S.O. and M.E.R. acknowledge the computer time provided by HPCI on the Oakbridge-CX cluster in the Information Technology Center, The University of Tokyo, under the Grant No. hp210246 of the "HPCI Infectious Disease including COVID-19 Research Access: Urgent Call" and by the Scientific Computing section of Research Support Division at OIST. A.M. thanks the financial support from the Compagnia di San Paolo, Project MINIERA No. I34I20000380007.

AUTHOR DECLARATIONS

Conflict of Interest

The authors have no conflict of interest to disclose.

DATA AVAILABILITY

The data that support the findings of this study are available from the corresponding author upon reasonable request.

APPENDIX: LIST OF PHYSICAL AND CHEMICAL PARAMETERS

The list of all physical and chemical parameters involved in our mathematical model is provided in Table II.

TABLE II. List of physical and chemical parameters assumed in the present work.

Mean ambient temperature	T_a	25 °C
Crystallization (or efflorescence) RH	CRH	45%
Deliquescence RH	DRH	75%
Quiescent ambient RH (wet)	RH_a	60%
Quiescent ambient RH (dry)	RH_a	30%
Density of liquid water	ρ_w	9.97×10^2 kg/m^3
Density of soluble aerosol part (NaCl)	ρ_s	2.2×10^3 kg/m^3
Density of insoluble aerosol part (mucus)	ρ_u	1.5×10^3 kg/m^3
Mass fraction of soluble material (NaCl) with respect to the total dry nucleus	ε_m	0.75
Mass fraction of dry nucleus with respect to the total droplet	C	1 %
Specific gas constant of water vapor	R_v	4.6×10^2 J/(kg K)
Diffusivity of water vapor	D_v	2.5×10^{-5} m^2/s
Density of air	ρ	1.18 kg/m^3
Kinematic viscosity of air	ν	1.8×10^{-5} m^2/s
Heat conductivity of dry air	k_a	2.6×10^{-2} W/K m
Latent heat for evaporation of liquid water	L_w	2.3×10^6 J/kg
Saturation vapor pressure	e_{sat}	0.616 kPa
Droplet condensational growth rate	C_R	1.5×10^{-10} m^2/s
Surface tension between moist air and salty water	σ	7.6×10^{-2} J/m^2
Molar mass of NaCl	M_s	5.9×10^{-2} kg/mol
Molar mass of water	M_w	1.8×10^{-2} kg/mol
Molar mass of water vapor and molar mass of dry air ratio	ε	0.61

REFERENCES

[1]S. Asadi, N. Bouvier, A. S. Wexler, and W. D. Ristenpart, "The coronavirus pandemic and aerosols: Does COVID-19 transmit via expiratory particles?," Aerosol Sci. Technol. **54**, 635–638 (2020).
[2]R. Mittal, R. Ni, and J.-H. Seo, "The flow physics of COVID-19," J. Fluid Mech. **894**, F2 (2020).
[3]K. L. Chong, C. S. Ng, N. Hori, R. Yang, R. Verzicco, and D. Lohse, "Extended lifetime of respiratory droplets in a turbulent vapor puff and its implications on airborne disease transmission," Phys. Rev. Lett. **126**, 034502 (2021).
[4]L. Bourouiba, "Turbulent gas clouds and respiratory pathogen emissions: Potential implications for reducing transmission of COVID-19," JAMA **323**, 1837–1838 (2020).
[5]R. Zhang, Y. Li, A. L. Zhang, Y. Wang, and M. J. Molina, "Identifying airborne transmission as the dominant route for the spread of COVID-19," Proc. Natl. Acad. Sci. U. S. A. **117**, 14857–14863 (2020).
[6]J. Dehning, J. Zierenberg, F. P. Spitzner, M. Wibral, J. P. Neto, M. Wilczek, and V. Priesemann, "Inferring change points in the spread of COVID-19 reveals the effectiveness of interventions," Science **369**, eabb9789 (2020).
[7]C. P. Cummins, O. J. Ajayi, F. V. Mehendale, R. Gabl, and I. M. Viola, "The dispersion of spherical droplets in source–sink flows and their relevance to the COVID-19 pandemic," Phys. Fluids **32**, 083302 (2020).
[8]C. M. Hafner, "The spread of the COVID-19 pandemic in time and space," Int. J. Environ. Res. Public Health **17**, 3827 (2020).
[9]S. Chaudhuri, S. Basu, P. Kabi, V. R. Unni, and A. Saha, "Modeling the role of respiratory droplets in COVID-19 type pandemics," Phys. Fluids **32**, 063309 (2020).
[10]J. Wang, M. Alipour, G. Soligo, A. Roccon, M. De Paoli, F. Picano, and A. Soldati, "Short-range exposure to airborne virus transmission and current guidelines," Proc. Natl. Acad. Sci. U. S. A. **118**, e2105279118 (2021).
[11]M. Rosti, S. Olivieri, M. Cavaiola, A. Seminara, and A. Mazzino, "Fluid dynamics of COVID-19 airborne infection suggests urgent data for a scientific design of social distancing," Sci. Rep. **10**, 1–9 (2020).
[12]Z.-Y. Ge, L. M. Yang, J.-J. Xia, X.-H. Fu, and Y.-Z. Zhang, "Possible aerosol transmission of COVID-19 and special precautions in dentistry," J. Zhejiang Univ.-Sci. B **21**, 361 (2020).
[13]L. Zhao, Y. Qi, P. Luzzatto-Fegiz, Y. Cui, and Y. Zhu, "COVID-19: Effects of environmental conditions on the propagation of respiratory droplets," Am. Chem. Soc. **20**, 7744–7750 (2020).
[14]N. Guerrero, J. M. Brito, and P. Cornejo, "COVID-19. transport of respiratory droplets in a microclimatologic urban scenario," medRxiv (2020).
[15]X. Li, C. M. Mak, K. W. Ma, and H. M. Wong, "Evaluating flow-field and expelled droplets in the mockup dental clinic during the COVID-19 pandemic," Phys. Fluids **33**, 047111 (2021).
[16]B. Blocken, F. Malizia, T. van Druenen, and T. Marchal, "Towards aerodynamically equivalent COVID-19 1.5 m social distancing for walking and running" (Questions and Answers) (unpublished), available at http://www.urbanphysics.net/COVID19.html; accessed 21 April 2020.
[17]Y. Feng, T. Marchal, T. Sperry, and H. Yi, "Influence of wind and relative humidity on the social distancing effectiveness to prevent COVID-19 airborne transmission: A numerical study," J. Aerosol Sci. **147**, 105585 (2020).
[18]A. Ahlawat, A. Wiedensohler, S. K. Mishra *et al.*, "An overview on the role of relative humidity in airborne transmission of SARS-CoV-2 in indoor environments," Aerosol Air Qual. Res. **20**, 1856–1861 (2020).
[19]A. Issakhov, Y. Zhandaulet, P. Omarova, A. Alimbek, A. Borsikbayeva, and A. Mustafayeva, "A numerical assessment of social distancing of preventing airborne transmission of COVID-19 during different breathing and coughing processes," Sci. Rep. **11**, 1–39 (2021).

[20]S. Balusamy, S. Banerjee, and K. C. Sahu, "Lifetime of sessile saliva droplets in the context of SARS-CoV-2," Int. Commun. Heat Mass Transfer **123**, 105178 (2021).
[21]M. Rosti, M. Cavaiola, S. Olivieri, A. Seminara, and A. Mazzino, "Turbulence role in the fate of virus-containing droplets in violent expiratory events," Phys. Rev. Res. **3**, 013091 (2021).
[22]R. C. Schroter, "Social distancing for COVID-19: Is 2 metres far enough?," BMJ **369**, m2010 (2020).
[23]C. Sun and Z. Zhai, "The efficacy of social distance and ventilation effectiveness in preventing COVID-19 transmission," Sustainable Cities Soc. **62**, 102390 (2020).
[24]M. Qian and J. Jiang, "COVID-19 and social distancing," J. Public Health **2020**, 1–3.
[25]W. Lyu and G. L. Wehby, "Community use of face masks and COVID-19: Evidence from a natural experiment of state mandates in the us: Study examines impact on COVID-19 growth rates associated with state government mandates requiring face mask use in public," Health Affairs **39**, 1419–1425 (2020).
[26]S. Verma, M. Dhanak, and J. Frankenfield, "Visualizing the effectiveness of face masks in obstructing respiratory jets," Phys. Fluids **32**, 061708 (2020).
[27]H. K. Sra, A. Sandhu, and M. Singh, "Use of face masks in COVID-19," Indian J. Pediatr. **87**, 553–553 (2020).
[28]H. Ueki, Y. Furusawa, K. Iwatsuki-Horimoto, M. Imai, H. Kabata, H. Nishimura, and Y. Kawaoka, "Effectiveness of face masks in preventing airborne transmission of SARS-CoV-2," mSphere **5**, e00637-20 (2020).
[29]E. P. Fischer, M. C. Fischer, D. Grass, I. Henrion, W. S. Warren, and E. Westman, "Low-cost measurement of face mask efficacy for filtering expelled droplets during speech," Sci. Adv. **6**, eabd3083 (2020).
[30]R. V. W. Endersby, E. C. Y. Ho, A. O. Spencer, D. H. Goldstein, and E. Schubert, "Barrier devices for reducing aerosol and droplet transmission in COVID-19 patients: Advantages, disadvantages, and alternative solutions," Anesth. Analg. **131**, e121–e123 (2020).
[31]K. Asokan, B. Babu, and A. Jayadevan, "Barrier enclosure for airway management in COVID-19 pandemic," Indian J. Anaesth. **64**, 153 (2020).
[32]P. Laosuwan, A. Earsakul, P. Pannangpetch, and J. Sereeyotin, "Acrylic box versus plastic sheet covering on droplet dispersal during extubation in COVID-19 patients," Anesth. Analg. **131**(2), e106–e108 (2020).
[33]E. A. Fried, G. Zhou, R. Shah, D. W. Shin, A. Shah, D. Katz, and G. W. Burnett, "Barrier devices, intubation, and aerosol mitigation strategies: Personal protective equipment in the time of coronavirus disease 2019," Anesth. Analg. **132**(1), 38–45 (2020).
[34]G. Boffetta and A. Mazzino, "Incompressible Rayleigh–Taylor turbulence," Annu. Rev. Fluid Mech. **49**, 119–143 (2017).
[35]M. L. Salby, *Fundamentals of Atmospheric Physics* (Elsevier, 1996).
[36]J. Monteith and M. Unsworth, *Principles of Environmental Physics: Plants, Animals, and the Atmosphere* (Academic Press, 2013).
[37]M. R. Maxey and J. J. Riley, "Equation of motion for a small rigid sphere in a nonuniform flow," Phys. Fluids **26**, 883–889 (1983).
[38]L.-P. Wang and M. R. Maxey, "Settling velocity and concentration distribution of heavy particles in homogeneous isotropic turbulence," J. Fluid Mech. **256**, 27–68 (1993).
[39]L. Bourouiba, E. Dehandschoewercker, and J. W. Bush, "Violent expiratory events: On coughing and sneezing," J. Fluid Mech. **745**, 537–563 (2014).
[40]H. R. Pruppacher and J. D. Klett, *Microphysics of Clouds and Precipitation* (Springer Netherlands, 2010).
[41]A. Celani, G. Falkovich, A. Mazzino, and A. Seminara, "Droplet condensation in turbulent flows," Europhys. Lett. **70**, 775 (2005).
[42]A. Celani, A. Mazzino, and M. Tizzi, "The equivalent size of cloud condensation nuclei," New J. Phys. **10**, 075021 (2008).
[43]A. Celani, A. Mazzino, and M. Tizzi, "Droplet feedback on vapor in a warm cloud," Int. J. Mod. Phys. B **23**, 5434–5443 (2009).
[44]J. Duguid, "The size and the duration of air-carriage of respiratory droplets and droplet-nuclei," Epidemiol. Infect. **44**, 471–479 (1946).
[45]L. Morawska, G. Johnson, Z. Ristovski, M. Hargreaves, K. Mengersen, S. Corbett, C. Y. H. Chao, Y. Li, and D. Katoshevski, "Size distribution and sites of origin of droplets expelled from the human respiratory tract during expiratory activities," J. Aerosol Sci. **40**, 256–269 (2009).
[46]J. K. Gupta, C.-H. Lin, and Q. Chen, "Flow dynamics and characterization of a cough," Indoor Air **19**, 517–525 (2009).
[47]M. E. Rosti and L. Brandt, "Numerical simulation of turbulent channel flow over a viscous hyper-elastic wall," J. Fluid Mech. **830**, 708–735 (2017).
[48]M. E. Rosti, S. Olivieri, A. A. Banaei, L. Brandt, and A. Mazzino, "Flowing fibers as a proxy of turbulence statistics," Meccanica **55**, 357– 370 (2020).
[49]M. Cavaiola, S. Olivieri, and A. Mazzino, "The assembly of freely moving rigid fibres measures the flow velocity gradient tensor," J. Fluid Mech. **894**, A25 (2020).
[50]M. E. Rosti, Z. Ge, S. S. Jain, M. S. Dodd, and L. Brandt, "Droplets in homogeneous shear turbulence," J. Fluid Mech. **876**, 962–984 (2019).
[51]M. E. Rosti and L. Brandt, "Increase of turbulent drag by polymers in particle suspensions," Phys. Rev. Fluids **5**, 041301 (2020).
[52]S. Olivieri, L. Brandt, M. E. Rosti, and A. Mazzino, "Dispersed fibers change the classical energy budget of turbulence via nonlocal transfer," Phys. Rev. Lett. **125**, 114501 (2020).
[53]A. Mazzino and M. E. Rosti, "Unraveling the secrets of turbulence in a fluid puff," Phys. Rev. Lett. **127**, 094501 (2021).
[54]T. Kajishima, T. Satoshi, H. HAMASAKI, and Y. MIYAKE, "Turbulence structure of particle-laden flow in a vertical plane channel due to vortex shedding," JSME Int. J., Ser. B **44**, 526–535 (2001).